The Astrophysical Journal Supplement Series, 167:334–342, 2006 December
© 2006. The American Astronomical Society. All rights reserved. Printed in U.S.A.

RADIATIVE RECOMBINATION DATA FOR MODELING DYNAMIC FINITE-DENSITY PLASMAS

N. R. Badnell
Department of Physics, University of Strathclyde, Glasgow G4 0NG, UK
Received 2006 April 6; accepted 2006 August 13

ABSTRACT

We have calculated partial final-state resolved radiative recombination (RR) rate coefficients from the initial ground and metastable levels of all elements up to and including Zn, plus Kr, Mo, and Xe, for all isoelectronic sequences up to Na-like forming Mg-like. The data are archived according to the Atomic Data and Analysis Structure (ADAS) data class *adf48*, which spans a temperature range of $z^2(10^1$–$10^7)$ K, where z is the initial ion charge. Fits to total rate coefficients have been determined, for both the ground and metastable levels, and those for the ground are presented here. Comparison is made both with previous RR rate coefficients and with (background) ***R***-matrix photoionization cross sections. This RR database complements a dielectronic recombination (DR) database already produced, and both are being used to produce updated ionization balances for both (electron) collisionally ionized and photoionized plasmas.

Subject headings: atomic data — atomic processes — plasmas

Online material: machine-readable table

1. INTRODUCTION

Astrophysical and laboratory plasmas that are not in (local) thermodynamic equilibrium require a detailed modeling of their atomic and, sometimes, molecular reactions so as to determine the level populations and ionization balance of their constituents. These in turn are basic ingredients for the physical and spectral diagnostic modeling of stellar coronae, gaseous nebulae, supernova remnants, fusion plasmas, etc. At low particle densities, e.g., the "coronal approximation," ionization balance is between total ground state dielectronic plus radiative recombination and ground state ionization by electrons and/or photons, while level populations are determined by collisional excitation from the ground state and radiation to all possible lower states. As the particle density increases, a separation between the two is no longer possible and level populations, effective recombination and ionization rate coefficients, and ionization balance are determined by solving the collisional–radiative population rate equations (Bates et al. 1962; Burgess & Summers 1969; Summers et al. 2006). Furthermore, even at the low densities found in gaseous nebulae, for example, the populations of ions of C, N, and O that have fine-structure levels in their ground term are not concentrated in the ground level. Recombination from excited levels within the ground term is quite different (smaller) compared to that for the ground level, due to the presence of additional autoionization pathways. Furthermore, transient plasmas such as solar flares do not have time to establish quasi-static equilibrium with the ground level and so require metastable levels (and the excited-state populations built on them) to be treated on an equal footing as the ground level when it comes to collisional–radiative modeling (Summers & Hooper 1983).

However, historically, total (zero-density) ground state recombination rate coefficients have dominated the literature—see, for example, those used by Shull & van Steenberg (1982), Arnaud & Rothenflug (1985), Péquignot et al. (1991), Arnaud & Raymond (1992), and Mazzotta et al. (1998). A systematic attempt to move beyond this picture has been described by Badnell et al. (2003), who focused on dielectronic recombination, but much of the discussion there is applicable to radiative recombination—deliberately so. Now, using AUTOSTRUCTURE (Badnell 1986), we have calculated partial final-state resolved radiative recombination (RR) rate coefficients from the initial ground and metastable levels of all elements up to and including Zn, plus Kr, Mo and Xe, for all isoelectronic sequences up to Na-like forming Mg-like. The data are archived according to the Atomic Data and Analysis Structure (ADAS) data class *adf48*[1] (Summers 2005). Fits to total RR rate coefficients have been determined, for both the ground and metastable levels, and those for the ground are presented here. All of the data are available online (Badnell 2006b), along with corresponding data for dielectronic recombination (DR; Badnell 2006a).

Previous work on RR has been summarized by Mazzotta et al. (1998). Since then, Gu (2003) has presented RR rate coefficients obtained using his Flexible Atomic Code (FAC) for Mg, Si, S, Ar, Ca, Fe, and Ni, for all isoelectronic sequences through to F-like forming Ne-like.

The time-reversed process of RR (plus DR) is photoionization (PI), indeed, our RR is determined from our direct photoionization cross sections on using the principle of detailed balance. We make comparison of our ground state to ground state and metastable photoionization cross sections of neutral atoms with those obtained from various ***R***-matrix calculations, by others, as the most severe test of our results. Similar ***R***-matrix data have been used by Nahar and coworkers (e.g., Nahar 1999) to form total (unified DR + RR) rate coefficients, and we make a comparison with it by combining our RR data with complementary DR data (Badnell 2006a).

The remainder of the paper is organized as follows: in § 2 we describe our methodology, in § 3 we present our results and make comparisons with the results of earlier works and then make some concluding remarks.

2. METHODOLOGY

2.1. *Theory*

We use the independent processes approximation so as to treat RR and DR separately. Interference between DR resonances and the RR background can safely be neglected, especially on integrating over resonance profiles (Pindzola et al. 1992). We use

[1] The historic ADAS dataclass file for RR is *adf08* but it is structured to handle RR to low-lying levels only, so as to supplement their population by electron-impact excitation.

AUTOSTRUCTURE (Badnell 1986) to calculate multiconfiguration intermediate coupling distorted-wave photoionization cross sections (Badnell & Seaton 2003). These are converted to RR cross sections using detailed balance. For elements beyond Zn, we use semirelativistic radial functions in place of the nonrelativistic ones used up until then (Pindzola & Badnell 1990).

2.2. *Atomic Details*

For each sequence, we used the same set of initial and final configurations as was done for ($\Delta n = 0$) DR (Badnell et al. 2003), i.e., we included configuration mixing in the initial N-electron, and final N- or $(N + 1)$-electron complexes for RR outside or into the initial complexes, respectively. Each inequivalent nl electron state was treated separately. Radial functions were determined using the Slater-Type-Orbital model potential option of AUTOSTRUCTURE, which generates (slightly, in this case) nonorthogonal orbitals. We follow Cowan (1981) in not imposing orthogonality and assuming the overlaps to be zero or unity, as appropriate. This is more of an issue for inner shell photoionization, where large relaxation effects occur for L-shell orbitals following K-shell photoionization (see, e.g., Gorczyca et al. 2006). For recombination/ionization to/from the ground complex, we used the observed ionization potentials from NIST (version 3).[2] Energy adjustments were made to the diagonal of the LS coupling Hamiltonian before recoupling to, and diagonalization of, the intermediate coupling Hamiltonian. Finally, to determine total RR and/or DR rate coefficients, we sum over only final states that are stable against autoionization.

2.3. *Numerics*

Cross sections were calculated at zero electron energy and then on a z-scaled logarithmic energy mesh with 3 points per decade spanning $(2.1 \times 10^{-6}$–$1 \times 10^{2})z^2$ ryd, where z is the charge of the ion before/after recombination/photoionization. Tests were also made using 5 points per decade. The length gauge is used at low energies, progressively and automatically switching to velocity and then acceleration as the energy increases so as to maintain numerical accuracy, but not before the succeeding gauge has converged to the preceding one. Cross sections at higher energies were determined by extrapolation as $E^{-l-7/2}$ (for PI), where l is the orbital angular momentum of the bound orbital (Fano & Cooper 1968). Rate coefficients were determined over $(10^{1}$–$10^{7})z^2$ K and so are not particularly sensitive to the exact form used for the extrapolation of the cross sections. With many thousands of individual partial rate coefficients to be determined, a fast and accurate Maxwellian convolution method is desirable. We use a variant of that due to Burgess (1964), viz., a 5 point Newton-Coates quadrature on a doubling energy mesh, with a 4 point Lagrange interpolation formula to convert from the initial logarithmic energy mesh, completed by an exponential integral. By using a z-scaled minimum temperature we can use a fixed maximum value for the principal quantum number, viz., 1000, and orbital angular momentum, viz., 200. We use analytic hydrogenic radial integrals for $l \geq 4$, making use of the fast, accurate, recurrence relations of Burgess (1964). All resultant partial RR rate coefficients are designed to be numerically accurate to 3 significant figures.

2.4. *Database Details*

The processing of photoionization cross sections from AUTOSTRUCTURE is carried out using the ADASRR code. The output of ADASRR is similar in nature to the ADASDR code used for DR (Badnell et al. 2003), i.e., the ADAS *adf48* file that it writes for RR is very similar in structure to the *adf09* file for DR (Summers 2005). Namely, for each initial level (ground plus metastables) there is a progressive bundling over final outer quantum numbers as n increases. Partial RR rate coefficients to low-lying levels (those with $n \leq 8$) are fully J-resolved, then bundled-nl ($n \leq 10$) and bundled-n ($n < 1000$), but each with a fully J_c-resolved core. Finally, total RR rate coefficients are written for each specified initial ground and metastable level. The full set of RR data—partials (*adf48* files) and totals (fit coefficients)—is available online (Badnell 2006b), alongside the DR data (Badnell 2006a), and it is also part of the ADAS distribution. (OPEN_ADAS, a public access version of ADAS is scheduled to come online in the summer of 2006, sponsored and hosted by the International Atomic Energy Agency.)

[2] NIST Atomic Spectral Database, version 3 (http://physics.nist.gov/PhysRefData/ASD).

2.5. *The Fit*

Total RR rate coefficients, for both ground and metastable initial levels, are fitted to the usual functional form (Verner & Ferland 1996; Gu 2003), viz.,

$$\alpha_{\rm RR}(T) = A\left[\sqrt{T/T_0}\left(1+\sqrt{T/T_0}\right)^{1-B}\left(1+\sqrt{T/T_1}\right)^{1+B}\right]^{-1}, \quad (1)$$

where, for low-charge ions, B is replaced as

$$B \rightarrow B + C\exp(-T_2/T). \quad (2)$$

Here $T_{0,1,2}$ are in units of temperature (K) and the rate coefficient $\alpha_{\rm RR}(T)$ is in units of cm^3 s^{-1}. (The units of A are also cm^3 s^{-1}, while B and C are dimensionless.) A nonlinear least-squares fit was used to determine the coefficients (A, B, $T_{0,1}$; C, T_2). The fits are accurate to better than 1% over $(10^{1}$–$10^{7})z^2$ K for multiply charged ions, 5% for singly and doubly ionized, and have the correct asymptotic forms outside of this temperature range.

3. RESULTS

Fit coefficients according to equations (1) and (2) are presented in Table 1 for total ground state RR rate coefficients for all elements up to and including Zn, plus Kr, Mo, and Xe, for all isoelectronic sequences up to Na-like forming Mg-like. Partial final-state resolved RR rate coefficients for initial ground and metastable levels are archived as ADAS *adf48* files (Summers 2005). Fits to total RR rate coefficients have been determined for initial metastable levels as well. All of the data are available online (Badnell 2006b), along with corresponding data for DR (Badnell 2006a).

3.1. *Photoionization Cross Sections*

The description of ground state photoionization of neutral atoms provides the most stringent test of the accuracy of our description of partial and high-temperature total RR rate coefficients.

In Figure 1 we compare photoionization cross sections of neutral O for the ground state to ground state and metastable transitions $O(^3P) \rightarrow O^+(^4S, ^2D, ^2P)$. We see that our AUTOSTRUCTURE results generally track the background ***R***-matrix cross sections of Butler & Zeippen (1990) quite closely, to within 7% at all energies for the O^+ ground state but somewhat larger (up to 20%) within 0.5 eV of threshold for the metastables.

In Figure 2 we make a similar comparison for neutral Na. This is an interesting system since it features a Cooper minimum (Fano

TABLE 1

Fit Coefficients for Total Ground State RR Rate Coefficients

Z	N	A	B	T_0	T_1	C	T_2
1.....	0	8.318(−11)	0.7472	2.965(0)	7.001(5)		
2.....	0	1.818(−10)	0.7492	1.017(1)	2.786(6)		
3.....	0	2.867(−10)	0.7493	2.108(1)	6.268(6)		
4.....	0	3.375(−10)	0.7475	4.628(1)	1.121(7)		
5.....	0	4.647(−10)	0.7484	6.142(1)	1.753(7)		
6.....	0	5.337(−10)	0.7485	9.502(1)	2.517(7)		
7.....	0	6.170(−10)	0.7481	1.316(2)	3.427(7)		
8.....	0	6.552(−10)	0.7470	1.951(2)	4.483(7)		
9.....	0	8.218(−10)	0.7491	2.046(2)	5.638(7)		
10.....	0	8.278(−10)	0.7470	2.991(2)	7.006(7)		
11.....	0	9.743(−10)	0.7488	3.217(2)	8.428(7)		
12.....	0	1.022(−09)	0.7476	4.098(2)	1.011(8)		
13.....	0	1.134(−09)	0.7482	4.619(2)	1.179(8)		
14.....	0	1.261(−09)	0.7488	5.068(2)	1.365(8)		
15.....	0	1.269(−09)	0.7472	6.495(2)	1.581(8)		
16.....	0	1.432(−09)	0.7485	6.688(2)	1.793(8)		
17.....	0	1.487(−09)	0.7489	7.847(2)	2.012(8)		
18.....	0	1.615(−09)	0.7483	8.433(2)	2.266(8)		
19.....	0	1.623(−09)	0.7473	1.024(3)	2.543(8)		
20.....	0	1.809(−09)	0.7490	1.025(3)	2.788(8)		
21.....	0	1.752(−09)	0.7470	1.303(3)	3.095(8)		
22.....	0	1.899(−09)	0.7476	1.348(3)	3.393(8)		
23.....	0	2.051(−09)	0.7490	1.389(3)	3.691(8)		
24.....	0	2.046(−09)	0.7476	1.638(3)	4.027(8)		
25.....	0	2.306(−09)	0.7499	1.546(3)	4.333(8)		
26.....	0	2.275(−09)	0.7481	1.836(3)	4.736(8)		
27.....	0	2.234(−09)	0.7461	2.190(3)	5.152(8)		
28.....	0	2.577(−09)	0.7497	1.949(3)	5.434(8)		
29.....	0	2.456(−09)	0.7477	2.414(3)	5.896(8)		
30.....	0	2.854(−09)	0.7491	2.125(3)	6.271(8)		
36.....	0	3.140(−09)	0.7485	3.537(3)	9.062(8)		
42.....	0	3.583(−09)	0.7474	5.008(3)	1.235(9)		
54.....	0	5.120(−09)	0.7493	6.912(3)	2.036(9)		
2.....	1	5.235(−11)	0.6988	7.301(0)	4.475(6)	0.0829	1.682(5)
3.....	1	9.349(−11)	0.6916	3.470(1)	7.329(6)	0.0351	6.293(5)
4.....	1	1.324(−10)	0.6806	8.525(1)	1.510(7)		
5.....	1	1.729(−10)	0.6776	1.552(2)	2.065(7)		
6.....	1	2.044(−10)	0.6742	2.647(2)	2.773(7)		
7.....	1	2.388(−10)	0.6732	3.960(2)	3.583(7)		
8.....	1	2.652(−10)	0.6705	5.842(2)	4.559(7)		
9.....	1	3.128(−10)	0.6712	7.227(2)	5.587(7)		
10.....	1	3.415(−10)	0.6706	9.552(2)	6.778(7)		
11.....	1	3.879(−10)	0.6718	1.133(3)	8.008(7)		
12.....	1	4.214(−10)	0.6713	1.396(3)	9.433(7)		
13.....	1	4.578(−10)	0.6707	1.673(3)	1.096(8)		
14.....	1	4.870(−10)	0.6697	2.026(3)	1.265(8)		
15.....	1	5.520(−10)	0.6724	2.146(3)	1.423(8)		
16.....	1	5.546(−10)	0.6692	2.754(3)	1.633(8)		
17.....	1	6.110(−10)	0.6712	2.956(3)	1.810(8)		
18.....	1	6.405(−10)	0.6698	3.425(3)	2.037(8)		
19.....	1	7.022(−10)	0.6721	3.602(3)	2.234(8)		
20.....	1	7.045(−10)	0.6693	4.391(3)	2.500(8)		
21.....	1	8.052(−10)	0.6750	4.198(3)	2.669(8)		
22.....	1	8.152(−10)	0.6728	4.937(3)	2.950(8)		
23.....	1	8.373(−10)	0.6711	5.622(3)	3.232(8)		
24.....	1	8.771(−10)	0.6722	6.118(3)	3.478(8)		
25.....	1	9.127(−10)	0.6717	6.691(3)	3.775(8)		
26.....	1	9.983(−10)	0.6754	6.651(3)	4.017(8)		
27.....	1	1.017(−09)	0.6738	7.469(3)	4.347(8)		
28.....	1	1.063(−09)	0.6744	7.979(3)	4.653(8)		
29.....	1	1.078(−09)	0.6736	8.924(3)	4.988(8)		
30.....	1	1.142(−09)	0.6750	9.193(3)	5.308(8)		
36.....	1	1.245(−09)	0.6716	1.601(4)	7.664(8)		
42.....	1	1.536(−09)	0.6764	2.012(4)	1.008(9)		
54.....	1	2.278(−09)	0.6872	2.680(4)	1.560(9)		

TABLE 1—*Continued*

Z	N	A	B	T_0	T_1	C	T_2
3.....	2	8.700(−12)	0.3640	1.470(2)	7.153(6)	0.1508	7.154(5)
4.....	2	1.861(−11)	0.4052	5.365(2)	2.254(7)		
5.....	2	3.251(−11)	0.4558	9.164(2)	1.749(7)		
6.....	2	4.798(−11)	0.4834	1.355(3)	1.872(7)		
7.....	2	6.245(−11)	0.4985	1.957(3)	2.177(7)		
8.....	2	8.193(−11)	0.5165	2.392(3)	2.487(7)		
9.....	2	9.958(−11)	0.5274	3.012(3)	2.896(7)		
10.....	2	1.186(−10)	0.5354	3.647(3)	3.365(7)		
11.....	2	1.393(−10)	0.5433	4.258(3)	3.872(7)		
12.....	2	1.602(−10)	0.5492	4.944(3)	4.434(7)		
13.....	2	1.761(−10)	0.5514	5.962(3)	5.081(7)		
14.....	2	2.017(−10)	0.5588	6.494(3)	5.693(7)		
15.....	2	2.190(−10)	0.5607	7.591(3)	6.396(7)		
16.....	2	2.362(−10)	0.5615	8.776(3)	7.208(7)		
17.....	2	2.594(−10)	0.5663	9.623(3)	7.952(7)		
18.....	2	2.812(−10)	0.5686	1.063(4)	8.779(7)		
19.....	2	3.046(−10)	0.5712	1.160(4)	9.639(7)		
20.....	2	3.250(−10)	0.5743	1.276(4)	1.051(8)		
21.....	2	3.366(−10)	0.5721	1.473(4)	1.163(8)		
22.....	2	3.658(−10)	0.5767	1.540(4)	1.250(8)		
23.....	2	3.815(−10)	0.5761	1.718(4)	1.368(8)		
24.....	2	3.963(−10)	0.5760	1.914(4)	1.479(8)		
25.....	2	4.386(−10)	0.5838	1.888(4)	1.556(8)		
26.....	2	4.458(−10)	0.5802	2.155(4)	1.701(8)		
27.....	2	4.629(−10)	0.5805	2.352(4)	1.831(8)		
28.....	2	4.901(−10)	0.5836	2.460(4)	1.937(8)		
29.....	2	5.041(−10)	0.5828	2.701(4)	2.082(8)		
30.....	2	5.258(−10)	0.5832	2.882(4)	2.221(8)		
36.....	2	6.300(−10)	0.5851	4.346(4)	3.140(8)		
42.....	2	8.161(−10)	0.5972	5.082(4)	4.054(8)		
54.....	2	1.082(−09)	0.6049	8.335(4)	6.391(8)		
4.....	3	1.793(−10)	0.7669	8.938(−01)	2.138(6)	0.0310	1.382(4)
5.....	3	3.417(−10)	0.7512	3.604(0)	2.821(6)	0.0351	1.295(7)
6.....	3	1.120(−10)	0.6737	1.115(2)	5.938(6)		
7.....	3	1.533(−10)	0.6682	1.823(2)	7.751(6)		
8.....	3	1.724(−10)	0.6556	3.372(2)	1.030(7)		
9.....	3	2.244(−10)	0.6574	4.147(2)	1.268(7)		
10.....	3	2.755(−10)	0.6586	5.102(2)	1.535(7)		
11.....	3	3.171(−10)	0.6576	6.526(2)	1.848(7)		
12.....	3	3.445(−10)	0.6553	8.693(2)	2.196(7)		
13.....	3	3.916(−10)	0.6565	1.025(3)	2.544(7)		
14.....	3	4.633(−10)	0.6602	1.088(3)	2.896(7)		
15.....	3	4.972(−10)	0.6581	1.329(3)	3.346(7)		
16.....	3	5.511(−10)	0.6598	1.492(3)	3.755(7)		
17.....	3	6.038(−10)	0.6611	1.670(3)	4.213(7)		
18.....	3	6.557(−10)	0.6624	1.868(3)	4.693(7)		
19.....	3	7.052(−10)	0.6613	2.094(3)	5.246(7)		
20.....	3	7.848(−10)	0.6644	2.173(3)	5.749(7)		
21.....	3	8.463(−10)	0.6653	2.355(3)	6.304(7)		
22.....	3	9.040(−10)	0.6666	2.565(3)	6.864(7)		
23.....	3	9.483(−10)	0.6655	2.859(3)	7.531(7)		
24.....	3	9.718(−10)	0.6643	3.285(3)	8.221(7)		
25.....	3	1.065(−09)	0.6668	3.327(3)	8.827(7)		
26.....	3	1.186(−09)	0.6713	3.253(3)	9.392(7)		
27.....	3	1.181(−09)	0.6681	3.839(3)	1.023(8)		
28.....	3	1.259(−09)	0.6699	3.991(3)	1.094(8)		
29.....	3	1.249(−09)	0.6668	4.697(3)	1.181(8)		
30.....	3	1.381(−09)	0.6705	4.543(3)	1.249(8)		
36.....	3	1.674(−09)	0.6723	6.836(3)	1.776(8)		
42.....	3	1.926(−09)	0.6717	9.982(3)	2.408(8)		
54.....	3	2.883(−09)	0.6818	1.355(4)	3.811(8)		
5.....	4	1.998(−09)	0.8277	1.269(−02)	1.016(6)	0.0901	3.058(4)
6.....	4	2.067(−09)	0.8012	1.643(−01)	2.172(6)	0.0427	6.341(4)
7.....	4	7.923(−10)	0.7768	3.750(0)	3.468(6)	0.0223	7.206(4)
8.....	4	3.955(−09)	0.7813	6.821(−01)	5.076(6)		

TABLE 1—*Continued*

Z	*N*	*A*	*B*	T_0	T_1	*C*	T_2
9.....	4	3.298(−09)	0.7702	2.103(0)	6.441(6)		
10.....	4	2.557(−09)	0.7601	6.293(0)	8.091(6)		
11.....	4	1.654(−09)	0.7508	2.276(1)	9.950(6)		
12.....	4	3.989(−10)	1.0231	2.601(1)	1.227(7)		
13.....	4	1.578(−09)	0.7394	6.157(1)	1.427(7)		
14.....	4	1.851(−09)	0.7384	6.906(1)	1.644(7)		
15.....	4	1.543(−09)	0.7315	1.330(2)	1.926(7)		
16.....	4	1.740(−09)	0.7303	1.494(2)	2.193(7)		
17.....	4	2.027(−09)	0.7307	1.541(2)	2.470(7)		
18.....	4	2.165(−09)	0.7307	1.801(2)	2.753(7)		
19.....	4	2.224(−09)	0.7299	2.212(2)	3.069(7)		
20.....	4	2.421(−09)	0.7278	2.438(2)	3.424(7)		
21.....	4	2.253(−09)	0.7253	3.425(2)	3.802(7)		
22.....	4	2.463(−09)	0.7249	3.638(2)	4.164(7)		
23.....	4	2.660(−09)	0.7253	3.897(2)	4.538(7)		
24.....	4	2.747(−09)	0.7251	4.436(2)	4.921(7)		
25.....	4	2.589(−09)	0.7216	5.887(2)	5.400(7)		
26.....	4	3.322(−09)	0.7264	4.563(2)	5.746(7)		
27.....	4	3.885(−09)	0.7301	4.100(2)	6.101(7)		
28.....	4	3.531(−09)	0.7260	5.650(2)	6.627(7)		
29.....	4	3.862(−09)	0.7272	5.631(2)	7.100(7)		
30.....	4	4.233(−09)	0.7283	5.568(2)	7.545(7)		
36.....	4	4.645(−09)	0.7261	1.018(3)	1.083(8)		
42.....	4	6.974(−09)	0.7318	9.622(2)	1.438(8)		
54.....	4	1.052(−08)	0.7363	1.319(3)	2.321(8)		
6.....	5	2.995(−09)	0.7849	6.670(−03)	1.943(6)	0.1597	4.955(4)
7.....	5	2.410(−09)	0.7948	1.231(−01)	3.016(6)	0.0774	1.016(5)
8.....	5	2.501(−09)	0.7844	5.235(−01)	4.470(6)	0.0447	1.642(5)
9.....	5	2.236(−09)	0.7725	1.828(0)	5.982(6)	0.0319	2.529(5)
10.....	5	1.127(−09)	0.7556	1.311(1)	8.047(6)	0.0250	2.771(5)
11.....	5	4.040(−09)	0.7665	2.908(0)	1.043(7)		
12.....	5	3.859(−09)	0.7579	5.587(0)	1.235(7)		
13.....	5	2.284(−09)	0.7480	2.178(1)	1.460(7)		
14.....	5	1.688(−09)	0.7390	5.549(1)	1.716(7)		
15.....	5	1.948(−09)	0.7375	6.372(1)	1.947(7)		
16.....	5	1.702(−09)	0.7301	1.138(2)	2.253(7)		
17.....	5	1.655(−09)	0.7262	1.636(2)	2.543(7)		
18.....	5	1.780(−09)	0.7252	1.933(2)	2.837(7)		
19.....	5	2.079(−09)	0.7245	1.954(2)	3.156(7)		
20.....	5	2.019(−09)	0.7215	2.644(2)	3.506(7)		
21.....	5	2.055(−09)	0.7200	3.236(2)	3.860(7)		
22.....	5	1.959(−09)	0.7169	4.381(2)	4.258(7)		
23.....	5	2.131(−09)	0.7166	4.679(2)	4.637(7)		
24.....	5	2.302(−09)	0.7167	5.002(2)	5.030(7)		
25.....	5	2.450(−09)	0.7160	5.442(2)	5.456(7)		
26.....	5	2.199(−09)	0.7118	7.810(2)	5.946(7)		
27.....	5	2.654(−09)	0.7148	6.726(2)	6.351(7)		
28.....	5	2.660(−09)	0.7150	7.865(2)	6.761(7)		
29.....	5	2.679(−09)	0.7128	9.094(2)	7.300(7)		
30.....	5	2.916(−09)	0.7150	9.113(2)	7.726(7)		
36.....	5	3.422(−09)	0.7122	1.533(3)	1.107(8)		
42.....	5	4.461(−09)	0.7147	1.874(3)	1.481(8)		
54.....	5	5.917(−09)	0.7162	3.263(3)	2.390(8)		
7.....	6	6.387(−10)	0.7308	9.467(−02)	2.954(6)	0.2440	6.739(4)
8.....	6	2.096(−09)	0.7668	1.602(−01)	4.377(6)	0.1070	1.392(5)
9.....	6	1.468(−09)	0.7652	1.284(0)	6.039(6)	0.0664	2.235(5)
10.....	6	1.861(−09)	0.7593	2.504(0)	8.037(6)	0.0406	3.255(5)
11.....	6	1.077(−09)	0.7469	1.430(1)	1.018(7)	0.0289	3.593(5)
12.....	6	9.133(−10)	0.7353	3.674(1)	1.263(7)	0.0211	4.049(5)
13.....	6	4.100(−09)	0.7507	5.134(0)	1.603(7)		
14.....	6	2.100(−09)	0.7401	2.523(1)	1.842(7)		
15.....	6	1.763(−09)	0.7310	5.234(1)	2.117(7)		
16.....	6	1.518(−09)	0.7246	9.845(1)	2.390(7)		
17.....	6	1.440(−09)	0.7187	1.522(2)	2.712(7)		
18.....	6	1.464(−09)	0.7144	2.040(2)	3.025(7)		

TABLE 1—*Continued*

Z	*N*	*A*	*B*	T_0	T_1	*C*	T_2
19.....	6	1.461(−09)	0.7108	2.734(2)	3.371(7)		
20.....	6	1.532(−09)	0.7089	3.305(2)	3.713(7)		
21.....	6	1.432(−09)	0.7048	4.761(2)	4.102(7)		
22.....	6	1.458(−09)	0.7005	5.875(2)	4.526(7)		
23.....	6	1.532(−09)	0.7008	6.698(2)	4.908(7)		
24.....	6	1.567(−09)	0.6986	7.957(2)	5.340(7)		
25.....	6	1.642(−09)	0.6982	8.948(2)	5.767(7)		
26.....	6	1.659(−09)	0.6958	1.061(3)	6.253(7)		
27.....	6	1.672(−09)	0.6935	1.254(3)	6.763(7)		
28.....	6	1.744(−09)	0.6928	1.385(3)	7.245(7)		
29.....	6	2.128(−09)	0.6988	1.157(3)	7.589(7)		
30.....	6	1.805(−09)	0.6906	1.794(3)	8.293(7)		
36.....	6	2.330(−09)	0.6908	2.631(3)	1.171(8)		
42.....	6	2.791(−09)	0.6893	3.801(3)	1.583(8)		
54.....	6	3.626(−09)	0.6904	6.985(3)	2.542(8)		
8.....	7	6.622(−11)	0.6109	4.136(0)	4.214(6)	0.4093	8.770(4)
9.....	7	5.595(−10)	0.7083	1.462(0)	6.258(6)	0.1645	1.880(5)
10.....	7	8.321(−10)	0.7254	3.332(0)	8.696(6)	0.0921	3.044(5)
11.....	7	1.087(−09)	0.7284	6.132(0)	1.088(7)	0.0629	4.559(5)
12.....	7	7.515(−10)	0.7203	2.582(1)	1.355(7)	0.0436	5.691(5)
13.....	7	7.728(−10)	0.7152	4.818(1)	1.672(7)	0.0271	7.209(5)
14.....	7	7.532(−10)	0.7072	8.860(1)	1.997(7)	0.0185	6.949(5)
15.....	7	1.570(−09)	0.7190	4.177(1)	2.438(7)		
16.....	7	1.137(−09)	0.7080	1.099(2)	2.745(7)		
17.....	7	1.146(−09)	0.7033	1.593(2)	3.034(7)		
18.....	7	1.022(−09)	0.6948	2.747(2)	3.391(7)		
19.....	7	9.722(−10)	0.6898	4.087(2)	3.753(7)		
20.....	7	9.575(−10)	0.6843	5.634(2)	4.150(7)		
21.....	7	1.011(−09)	0.6827	6.726(2)	4.518(7)		
22.....	7	1.043(−09)	0.6798	8.226(2)	4.947(7)		
23.....	7	1.049(−09)	0.6763	1.032(3)	5.381(7)		
24.....	7	1.053(−09)	0.6736	1.278(3)	5.857(7)		
25.....	7	1.089(−09)	0.6713	1.488(3)	6.327(7)		
26.....	7	1.135(−09)	0.6705	1.691(3)	6.809(7)		
27.....	7	1.177(−09)	0.6687	1.921(3)	7.331(7)		
28.....	7	1.172(−09)	0.6652	2.320(3)	7.926(7)		
29.....	7	1.295(−09)	0.6672	2.319(3)	8.388(7)		
30.....	7	1.250(−09)	0.6640	2.899(3)	8.992(7)		
36.....	7	1.497(−09)	0.6596	4.992(3)	1.277(8)		
42.....	7	1.748(−09)	0.6593	7.627(3)	1.705(8)		
54.....	7	2.624(−09)	0.6641	1.134(4)	2.699(8)		
9.....	8	3.769(−11)	0.5559	1.091(1)	6.413(6)	0.4534	1.095(5)
10.....	8	1.773(−10)	0.6434	9.924(0)	8.878(6)	0.2205	2.292(5)
11.....	8	3.192(−10)	0.6726	1.640(1)	1.263(7)	0.1232	3.725(5)
12.....	8	4.031(−10)	0.6803	3.205(1)	1.626(7)	0.0764	5.399(5)
13.....	8	4.438(−10)	0.6789	6.204(1)	1.940(7)	0.0571	7.410(5)
14.....	8	4.615(−10)	0.6753	1.143(2)	2.377(7)	0.0356	8.595(5)
15.....	8	5.508(−10)	0.6748	1.501(2)	2.772(7)	0.0213	1.109(6)
16.....	8	8.773(−10)	0.6853	1.115(2)	3.386(7)		
17.....	8	7.522(−10)	0.6767	2.213(2)	3.678(7)		
18.....	8	6.805(−10)	0.6667	3.866(2)	4.062(7)		
19.....	8	6.633(−10)	0.6599	5.735(2)	4.447(7)		
20.....	8	6.699(−10)	0.6546	7.761(2)	4.861(7)		
21.....	8	6.581(−10)	0.6494	1.072(3)	5.292(7)		
22.....	8	6.854(−10)	0.6464	1.313(3)	5.733(7)		
23.....	8	7.140(−10)	0.6441	1.579(3)	6.195(7)		
24.....	8	6.832(−10)	0.6367	2.162(3)	6.770(7)		
25.....	8	7.236(−10)	0.6359	2.448(3)	7.264(7)		
26.....	8	7.556(−10)	0.6351	2.800(3)	7.742(7)		
27.....	8	7.582(−10)	0.6307	3.402(3)	8.406(7)		
28.....	8	7.889(−10)	0.6292	3.842(3)	8.956(7)		
29.....	8	8.107(−10)	0.6290	4.369(3)	9.503(7)		
30.....	8	8.533(−10)	0.6278	4.759(3)	1.011(8)		
36.....	8	1.033(−09)	0.6234	8.342(3)	1.417(8)		
42.....	8	1.256(−09)	0.6232	1.220(4)	1.882(8)		

TABLE 1—*Continued*

Z	*N*	*A*	*B*	T_0	T_1	*C*	T_2
54.....	8	1.688(−09)	0.6241	2.245(4)	2.986(8)		
10.....	9	1.295(−11)	0.3556	6.739(1)	7.563(6)	0.6472	1.598(5)
11.....	9	5.176(−11)	0.4811	7.751(1)	1.351(7)	0.3467	3.140(5)
12.....	9	1.249(−10)	0.5600	7.748(1)	2.015(7)	0.1917	5.139(5)
13.....	9	2.011(−10)	0.5984	1.013(2)	2.635(7)	0.1072	7.591(5)
14.....	9	2.468(−10)	0.6113	1.649(2)	3.231(7)	0.0636	9.837(5)
15.....	9	2.981(−10)	0.6173	2.372(2)	3.807(7)	0.0361	1.306(6)
16.....	9	3.384(−10)	0.6175	3.380(2)	4.347(7)	0.0225	1.672(6)
17.....	9	4.354(−10)	0.6262	3.604(2)	5.251(7)		
18.....	9	4.228(−10)	0.6181	5.880(2)	5.535(7)		
19.....	9	4.044(−10)	0.6099	9.347(2)	5.922(7)		
20.....	9	3.992(−10)	0.6025	1.362(3)	6.373(7)		
21.....	9	4.070(−10)	0.5968	1.819(3)	6.864(7)		
22.....	9	4.281(−10)	0.5954	2.234(3)	7.270(7)		
23.....	9	4.227(−10)	0.5885	3.007(3)	7.863(7)		
24.....	9	4.341(−10)	0.5846	3.714(3)	8.452(7)		
25.....	9	4.710(−10)	0.5863	4.081(3)	8.874(7)		
26.....	9	4.791(−10)	0.5823	4.967(3)	9.535(7)		
27.....	9	5.045(−10)	0.5808	5.617(3)	1.015(8)		
28.....	9	5.081(−10)	0.5766	6.786(3)	1.088(8)		
29.....	9	5.402(−10)	0.5769	7.375(3)	1.150(8)		
30.....	9	5.284(−10)	0.5705	9.182(3)	1.239(8)		
36.....	9	6.842(−10)	0.5709	1.489(4)	1.680(8)		
42.....	9	8.282(−10)	0.5708	2.249(4)	2.193(8)		
54.....	9	1.109(−09)	0.5712	4.285(4)	3.443(8)		
11.....	10	5.095(−12)	0.0000	3.546(2)	2.310(6)	0.9395	4.297(5)
12.....	10	1.345(−11)	0.1074	7.877(2)	7.925(7)	0.4631	5.027(5)
13.....	10	3.107(−11)	0.2854	8.207(2)	8.117(7)	0.2631	7.693(5)
14.....	10	5.134(−11)	0.3678	1.009(3)	8.514(7)	0.1646	1.084(6)
15.....	10	7.550(−11)	0.4244	1.206(3)	8.603(7)	0.1008	1.498(6)
16.....	10	9.565(−11)	0.4517	1.599(3)	9.252(7)	0.0612	1.986(6)
17.....	10	1.144(−10)	0.4665	2.108(3)	9.895(7)	0.0362	2.397(6)
18.....	10	1.313(−10)	0.4722	2.767(3)	1.066(8)	0.0208	2.725(6)
19.....	10	1.590(−10)	0.4867	3.096(3)	1.192(8)		
20.....	10	1.622(−10)	0.4804	4.449(3)	1.204(8)		
21.....	10	1.647(−10)	0.4734	6.182(3)	1.253(8)		
22.....	10	1.730(−10)	0.4687	7.898(3)	1.302(8)		
23.....	10	1.800(−10)	0.4650	9.950(3)	1.357(8)		
24.....	10	1.868(−10)	0.4603	1.233(4)	1.432(8)		
25.....	10	1.924(−10)	0.4562	1.514(4)	1.509(8)		
26.....	10	2.034(−10)	0.4548	1.751(4)	1.579(8)		
27.....	10	2.125(−10)	0.4518	2.042(4)	1.667(8)		
28.....	10	2.208(−10)	0.4504	2.355(4)	1.749(8)		
29.....	10	2.271(−10)	0.4464	2.753(4)	1.853(8)		
30.....	10	2.397(−10)	0.4458	3.040(4)	1.941(8)		
36.....	10	3.051(−10)	0.4446	5.297(4)	2.530(8)		
42.....	10	3.541(−10)	0.4350	8.882(4)	3.334(8)		
54.....	10	4.923(−10)	0.4400	1.645(5)	5.012(8)		
12.....	11	5.452(−11)	0.6845	5.637(0)	1.551(6)	0.3945	8.360(5)
13.....	11	3.171(−11)	0.4493	1.821(2)	3.529(7)	0.2642	7.190(5)
14.....	11	6.739(−11)	0.4931	2.166(2)	4.491(7)	0.1667	9.046(5)
15.....	11	1.128(−10)	0.5330	2.618(2)	4.963(7)	0.0994	1.244(6)
16.....	11	1.588(−10)	0.5584	3.350(2)	5.188(7)	0.0591	1.656(6)
17.....	11	1.790(−10)	0.5641	5.390(2)	5.733(7)	0.0340	2.038(6)
18.....	11	2.156(−10)	0.5708	7.027(2)	6.146(7)	0.0169	2.845(6)
19.....	11	2.516(−10)	0.5771	8.854(2)	6.829(7)		
20.....	11	2.527(−10)	0.5711	1.364(3)	6.926(7)		
21.....	11	2.578(−10)	0.5655	1.955(3)	7.157(7)		
22.....	11	2.711(−10)	0.5628	2.552(3)	7.416(7)		
23.....	11	2.792(−10)	0.5588	3.360(3)	7.736(7)		
24.....	11	3.003(−10)	0.5585	3.987(3)	8.062(7)		
25.....	11	3.197(−10)	0.5582	4.712(3)	8.394(7)		
26.....	11	3.133(−10)	0.5507	6.295(3)	9.035(7)		
27.....	11	3.340(−10)	0.5516	7.145(3)	9.384(7)		
28.....	11	3.626(−10)	0.5536	7.769(3)	9.785(7)		
29.....	11	3.761(−10)	0.5509	9.021(3)	1.036(8)		

TABLE 1—*Continued*

Z	*N*	*A*	*B*	T_0	T_1	*C*	T_2
30.....	11	3.885(−10)	0.5492	1.041(4)	1.095(8)		
36.....	11	4.936(−10)	0.5469	1.900(4)	1.455(8)		
42.....	11	6.295(−10)	0.5525	2.751(4)	1.846(8)		
54.....	11	8.258(−10)	0.5485	5.795(4)	2.911(8)		

NOTES.—See eqs. (1) and (2). The quantity *Z* denotes the nuclear charge, and *N* represents the number of electrons on the ion before recombination. The notation (*n*) stands for $\times 10^n$. Table 1 is also available in machine-readable form in the electronic edition of the *Astrophysical Journal Supplement*.

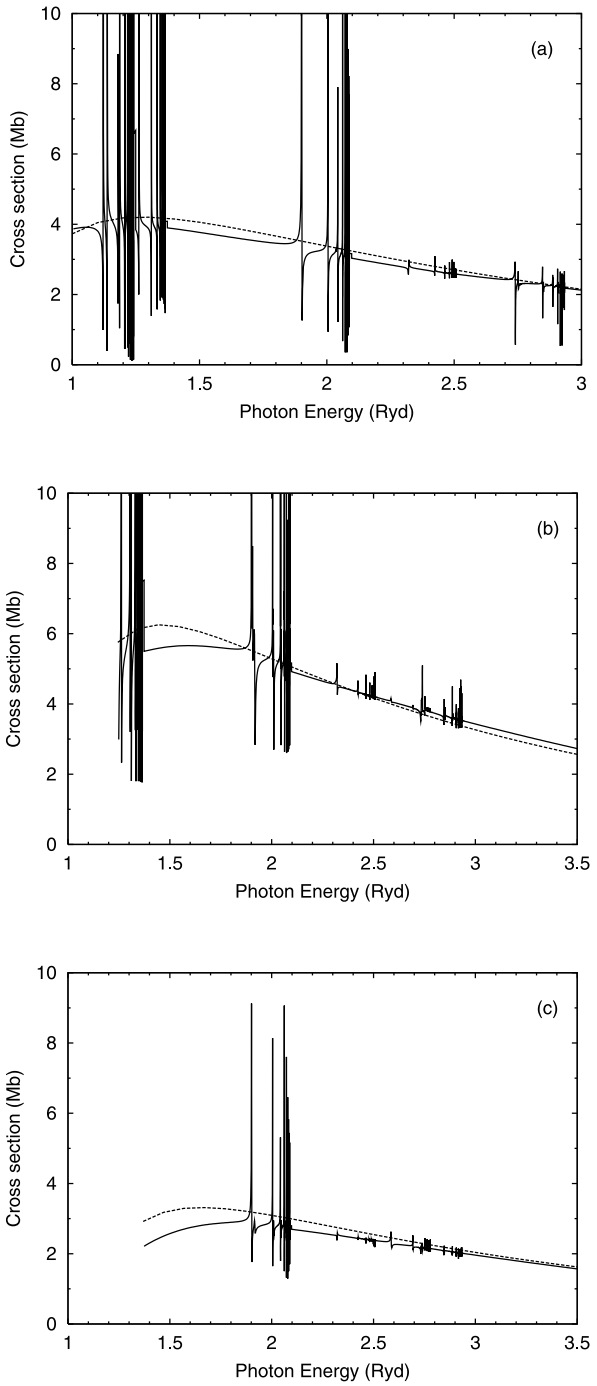

FIG. 1.—Photoionization of $O(^3P) \rightarrow O^+$: (*a*) ^4S, (*b*) ^2D, (*c*) ^2P. *Solid curve*: ***R***-matrix results (Butler & Zeippen 1990); *dashed curve*: present AUTOSTRUCTURE results.

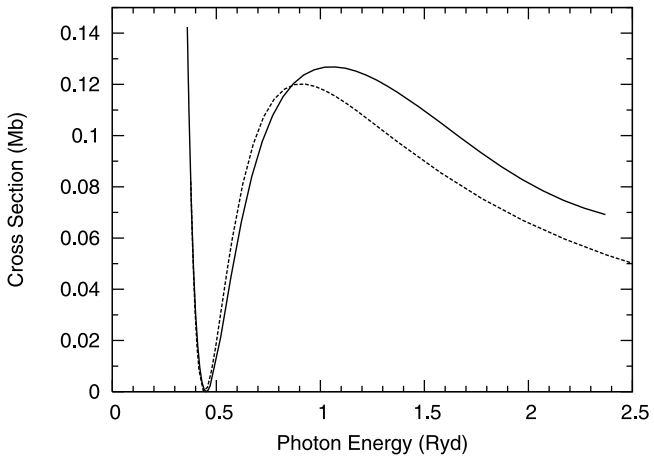

FIG. 2.—Photoionization of Na (3*s*). *Solid curve*, ***R***-matrix results (TOPbase; Cunto et al. 1993); *dashed curve*, present AUTOSTRUCTURE results.

& Cooper 1968). We see that our AUTOSTRUCTURE photoionization cross sections give a reasonable description of this feature, in comparison with the ***R***-matrix results of Butler & Mendoza (1983) and TOPbase[3] (Cunto et al. 1993).

Finally, in Figure 3 we look at the high-energy behavior of the Mg^+ photoionization cross section: we compare our energy-scaled AUTOSTRUCTURE cross sections with the Dirac-Hartree-Slater results of Verner & Yakovlev (1995) and the relativistic distorted wave (RDW) results of Zhang (1998). We see that at the high-energy cross sections of Verner & Yakovlev (1995) have still to reach their asymptotic form, of $E^{-7/2}$, while those of Zhang (1998) track the AUTOSTRUCTURE results closely. Analysis of the fitting form and parameters of Verner & Yakovlev (1995) shows that it will not reach asymptopia until $\sim 10^6$ ryd, which appears unphysically high. Similar disagreement is seen in other low-charge Na-like ions, the effect decreasing with increasing residual charge.

3.2. *Total Ground State Rate Coefficients*

In Figures 4 and 5 we illustrate an overview of total ground state RR rate coefficients, viz., the Mg isonuclear sequence and the F isoelectronic sequence. The change in behavior on moving from *K* to *L* and then *M* shells is clearly seen in the former and the characteristic high-temperature bump at low charges is seen in the latter. This is due to the highly nonhydrogenic screening of the wave functions for low-*nl* states, in low-charge many-electron ions, which dominate the recombination at high temperatures.

In Figure 6 we compare our F-like Ne and Mg rate coefficients from AUTOSTRUCTURE with those of Péquignot et al. (1991) and Gu (2003), respectively. The high-temperature limit on the validity of the simple functional form used by Péquignot et al. (1991) is a few times 10^4 K, but DR dominates thereon. The more general form, given by equations (1) and (2), does not suffer from this limitation. The comparison with the results of Gu (2003) for Mg illustrates the worst agreement found with his work, viz., about 10% in the vicinity of 5×10^4 K, and up to 20% at 10^8 K.

In Figure 7 we compare our Ne-like Na and Mg rate coefficients from AUTOSTRUCTURE with those of Verner & Ferland (1996). The latter are based on Opacity Project (TOPbase; Cunto et al. 1993) ***R***-matrix background photoionization cross sections at low energies and the Dirac-Hartree-Slater ones of Verner & Yakovlev (1995) at higher energies. We have already noted the good agreement between our low-energy (ground state) neutral

[3] See also http://vizier.u-strasbg.fr/topbase/topbase.html.

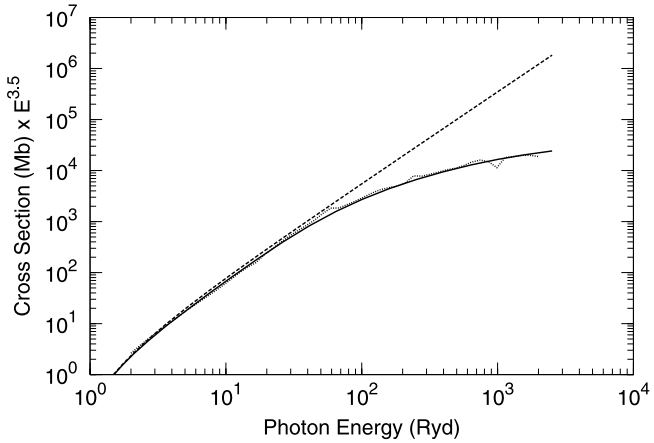

FIG. 3.—Scaled photoionization cross section of Mg^+ (3*s*). *Solid curve*, present AUTOSTRUCTURE results; *dashed curve*, Dirac-Hartree-Slater results of Verner & Yakovlev (1995); *dotted curve*, relativistic distorted wave results of Zhang (1998).

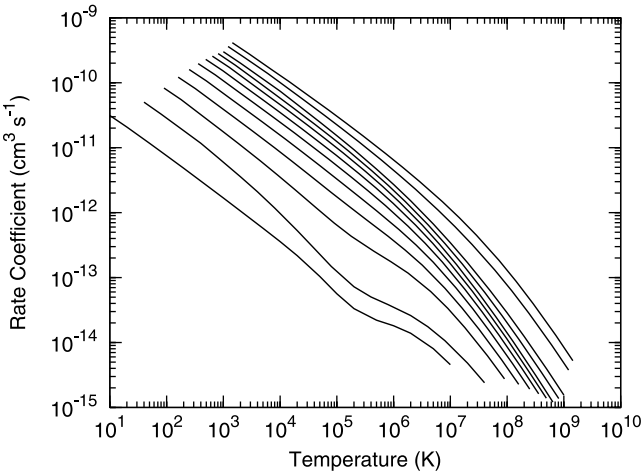

FIG. 4.—Total ground state RR rate coefficients for the Mg isonuclear sequence (present AUTOSTRUCTURE results). Curves for singly ionized to bare are shown, moving left to right.

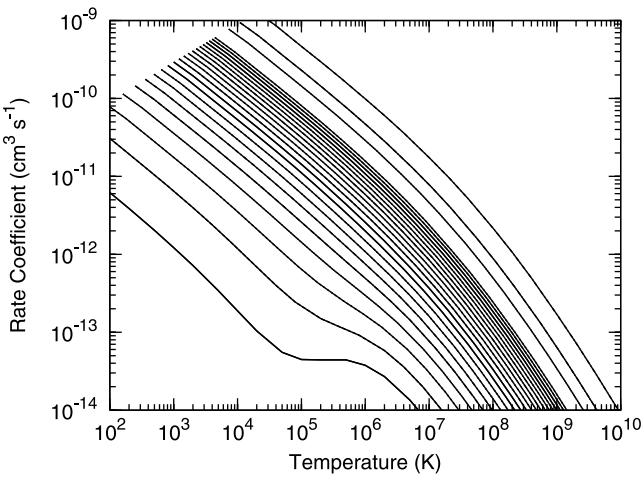

FIG. 5.—Total ground state RR rate coefficients for the F isoelectronic sequence (present AUTOSTRUCTURE results). Curves for Ne to Zn, plus Kr, Mo, and Xe, are shown, moving left to right.

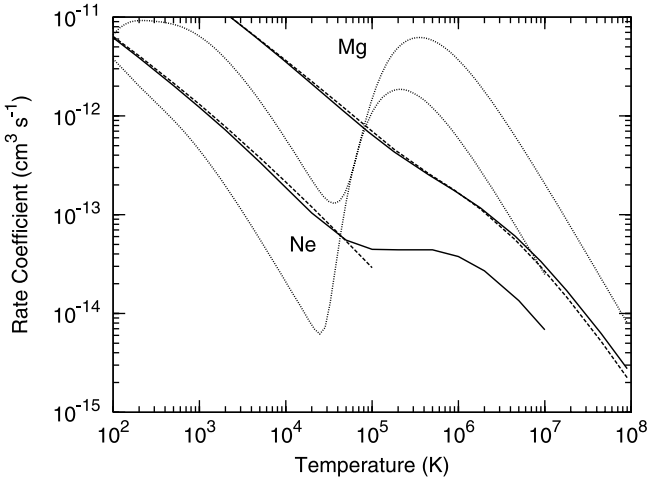

FIG. 6.—Total ground state rate coefficients for F-like Ne and Mg. *Solid curves*, present AUTOSTRUCTURE RR results; *dashed curves*, RR results of Péquignot et al. (1991) and Gu (2003) for Ne and Mg, respectively; *dotted curves*, DR results of Zatsarinny et al. (2006).

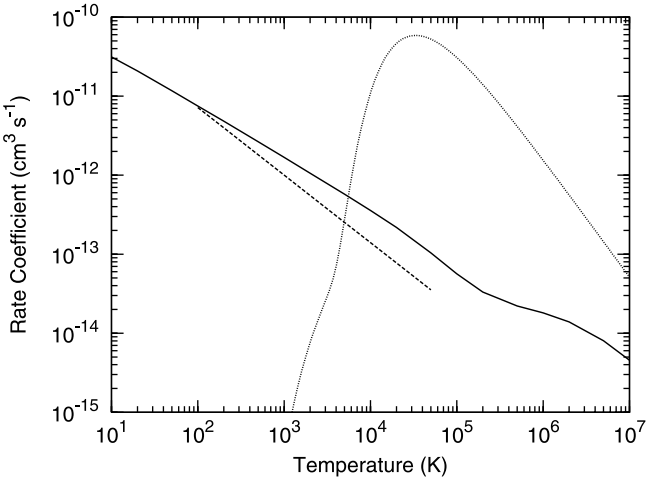

FIG. 8.—Total ground state rate coefficients for Mg^+. *Solid curves*, present AUTOSTRUCTURE RR results; *dashed curve*, RR results of Aldrovandi & Péquignot (1973); *dotted curves*, DR results of Altun et al. (2006).

Na photoionization cross sections and those from ***R***-matrix—those for Mg^+ show good agreement as well (not shown). We noted also that the high-energy Dirac-Hartree-Slater photoionization cross sections lie *above* those from AUTOSTRUCTURE. But, here, we see that the high-temperature RR rate coefficients of Verner & Ferland (1996) lie *below* our results—RR into the 3*s* dominates at high temperatures—which is puzzling. However, the rise of DR at 10^5 K postpones significant disagreement in the (DR + RR) total until $\sim 10^7$ K.

In Figure 8 we compare our Mg^+ rate coefficients from AUTOSTRUCTURE with the RR of Aldrovandi & Péquignot (1973; and used again by Shull & van Steenberg 1982 without modification), which still form the basis of recommended data for this ion (Mazzotta et al. 1998). Our RR results are 70% and a factor of 3 larger at 10^3 and 10^4 K, respectively, but DR dominates at the latter temperature, while it is negligible at the former. Gould (1978) also obtained results larger than those of Aldrovandi & Péquignot (1973) by a factor of 2 at 10^4 K. He speculated that Aldrovandi & Péquignot (1973) omitted capture to 3*p* and 3*d*. The results of Aldrovandi & Péquignot (1973) and Gould (1978) also make use of very restricted (near-threshold) photoionization cross section measurements by Ditchburn & Marr (1953). The results of Gould (1978) do not appear to have supplanted those of Aldrovandi & Péquignot (1973). Consequently, our new rate coefficient changes the ionization balance of Mg in many photoionized plasmas and affects Mg II emissivities noticeably (G. J. Ferland 2006, private communication), for example.

Finally, in Figure 9 we compare our total (DR + RR) rate coefficients from AUTOSTRUCTURE for O^{2+} with the (unified DR + RR) ***R***-matrix results of Nahar (1999). We also show separately the contribution from the present RR rate coefficients and the DR ones of Zatsarinny et al. (2004) taken from Badnell (2006a). At the high-temperature peak (2×10^5 K) the results of Nahar (1999) lie about 8% above the present ones and remain constantly so thereon. Below about 2×10^4 K the contribution from fine-structure DR separates the two results. The calculations of Nahar (1999) were carried out in *LS* coupling, and so this is contribution absent and her results track our RR results to within a few percent.

3.3. *Total Metastable Rate Coefficients*

In Figure 10 we present total rate coefficients from the ground and metastable levels of $O^{2+}(^3P_{0,1,2}, {}^1D_2, {}^1S_0, {}^5S_2)$. Fine-structure

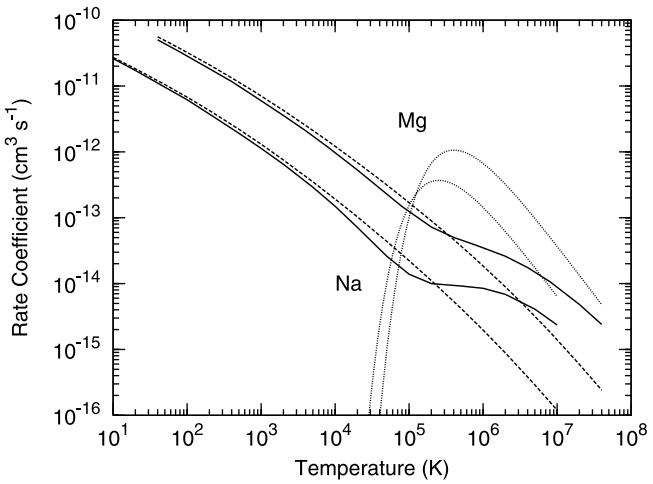

FIG. 7.—Total ground state rate coefficients for Ne-like Na and Mg. *Solid curves*, present AUTOSTRUCTURE RR results; *dashed curves*, RR results of Verner & Ferland (1996); *dotted curves*, DR results of Fu et al. (2006).

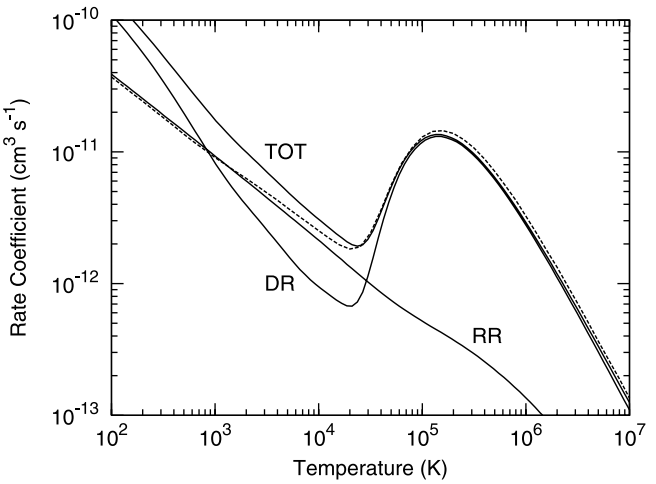

FIG. 9.—Total ground state rate coefficients for O^{2+}. *Solid curves*, RR (present), DR (Zatsarinny et al. 2004), and total (DR + RR) from AUTOSTRUCTURE; *dashed curve*, total (unified DR + RR) from ***R***-matrix (Nahar 1999).

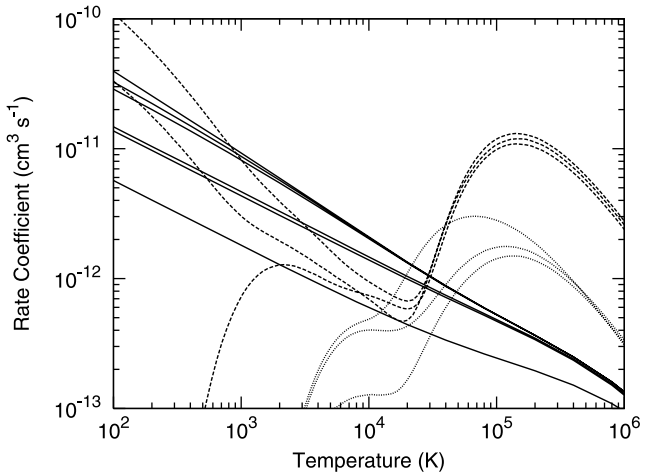

FIG. 10.—Total rate coefficients from the ground and metastable levels of O^{2+}($^3P_{0,1,2}$, $^1D_2$, $^1S_0$, $^5S_2$). *Solid curves*, RR, top-to-bottom at 10^5 K corresponds to increasing initial energy metastable; *dashed curves*, DR from levels of the ground term, top-to-bottom corresponds to increasing initial energy metastable; *dotted curves*, DR from the excited terms, bottom-to-top at 10^5 K corresponds to increasing initial energy metastable. All DR data are taken from Badnell (2006a) based on Zatsarinny et al. (2004).

splitting in the ^3P_J ground term only starts to affect RR at very low temperatures (~30% at 100 K). This is in contrast to DR, where the lower two levels are strongly enhanced by the fine-structure pathway(s) open to them, while the upper level only has a small low-temperature peak that never exceeds the RR contribution. RR onto excited terms is reduced distinctly by autoionization, compared to that for levels within a term. The $^1D_2$ and $^1S_0$ contributions are similarly sized, both for RR and the high-temperature DR peak (at 10^5 K). The $^5S_2$ RR contribution is the smallest, but its high-temperature DR peak exceeds that of the $^1D_2$ and $^1S_0$ initial states. The widely varying behaviors of DR and RR for ground and metastable levels is then reflected similarly in the temperature dependence of the (DR + RR) total recombination rate coefficients (not shown).

3.4. *Partial Rate Coefficients*

In Figures 11 and 12 we compare partial final-state resolved rate coefficients for recombination from the initial ground state

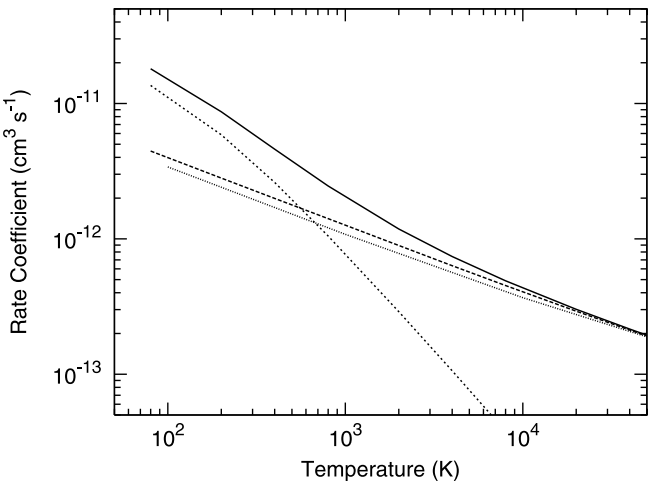

FIG. 11.—Partial recombination rate coefficients for O^{2+} to O^+ ground state to ground state. *Long-dashed curve*, RR (present); *short-dashed curve*, DR (Zatsarinny et al. 2004); *solid curve*, total (DR + RR) from AUTOSTRUCTURE; *dotted curve*, total (unified DR + RR) from ***R***-matrix (Nahar 1999).

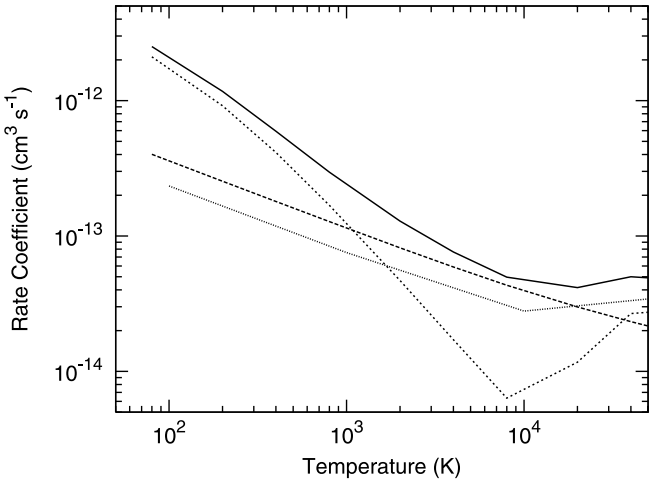

FIG. 12.—Partial recombination rate coefficients for O^{2+} ground state to O^+ $2s^22p^23p\,^4D$. *Long-dashed curve*, RR (present); *short-dashed curve*, DR (Zatsarinny et al. 2004); *solid curve*, total (DR + RR) from AUTOSTRUCTURE; *dotted curve*, total (unified DR + RR) from ***R***-matrix (Nahar 1999).

of O^{2+} to the $2s^22p^3\ ^4S_{3/2}$ and $2s^22p^23p^4D_J$ states of O^+, respectively, where we have summed over the fine-structure J of the ^4D term, for convenience of comparison. The DR is taken from the partial *adf09* files of Zatsarinny et al. (2004) archived by Badnell (2006a). As in the case of totals, we see that the partial DR is enhanced below ~1000 K by fine-structure transitions. The (*LS* coupling) ***R***-matrix results of Nahar (1999) lie 15% and 35% below our RR results for the ground and excited state, respectively, at temperatures below ~1000 K.

Recombination into the $2s^22p^23p\ ^4D_J$ states of O^+ is of interest because of the discrepancy in temperatures needed to model recombination line and forbidden line abundances in the Ring Nebula NGC 6720 (Garnett & Dinerstein 2001). The relevant recombination line (emissivity) is for the subsequent $3p\ ^4D$ to $3s\ ^4P$ transition at λ4661 in O II. The λ4661 emissivity used by Garnett & Dinerstein (2001) is based on the effective recombination rate coefficient of Storey (1994), whose calculations were carried out in *LS* coupling. We note (not shown) only a ≈10% enhancement of the zero-density noncascade partial sum (RR + DR) at 10^4 K, on going from *LS* to intermediate coupling. This enhancement becomes a factor of 2 down at 10^3 K, but it is probably too low a temperature to help resolve the discrepancy in the Ring Nebula. Interestingly, our partial sum (DR + RR) rate coefficient to $2s^22p^23p\ ^4D$ agrees to about 10% with the λ4661 effective recombination rate coefficient of Storey (1994) over the temperature range of 5×10^3–2×10^4 K for which he tabulates results. Since density effects are negligible for this line and the branching ratio for $3p\ ^4D$ to $3s\ ^4P$ is approximately unity, we infer that the cascade correction is not large. Work on a detailed revised λ4661 effective recombination rate coefficient is in progress (P. J. Storey 2006, private communication).

4. CONCLUDING REMARKS

We have outlined the database of RR rate coefficients that we have established using AUTOSTRUCTURE. Although we have highlighted some differences from previous results we have observed, the bulk of the ground state total data is in good accord with the extant. It is hoped that the availability of comprehensive partial final-state resolved and metastable totals will stimulate the advanced modeling of nonequilibrium astrophysical plasmas, viz., dynamic, finite density. Together with complementary data for DR, new ionization balances are already being determined for both

(electron) collisional (Bryans et al. 2006) and photoionized (G. J. Ferland 2006, private communication) plasmas.

I would like to thank Randall Smith and Daniel Péquignot for their interest in the partial and metastable RR rate coefficients, respectively. I would also like to thank Keith Butler for supplying his ***R***-matrix photoionization cross sections of O in numerical form and Hong Lin Zhang for recalculating his RDW Mg^+ 3*s* subshell photoionization cross section. This work was supported in part by PPARC grant PPA\G\S2003\00055 with the University of Strathclyde.

REFERENCES

Aldrovandi, S. M. V., & Péquignot, D. 1973, A&A, 25, 137
Altun, Z., Yumak, A., Badnell, N. R., Loch, S. D., & Pindzola, M. S. 2006, A&A, 447, 1165
Arnaud, M., & Raymond, J. C. 1992, ApJ, 398, 394
Arnaud, M., & Rothenflug, R. 1985, A&AS, 60, 425
Badnell, N. R. 1986, J. Phys. B, 19, 3827
———. 2006a, Fits for Total Dielectronic Recombination Rate Coefficients (http://amdpp.phys.strath.ac.uk/tamoc/DR/)
———. 2006b, Fits for Total Radiative Recombination Rate Coefficients (http://amdpp.phys.strath.ac.uk/tamoc/RR/)
Badnell, N. R., O'Mullane, M. G., Summers, H. P., Altun, Z., Bautista, M. A., Colgan, J., Gorczyca, T. W., Mitnik, D. M., Pindzola, M. S., & Zatsarinny, O. 2003, A&A, 406, 1151
Badnell, N. R., & Seaton, M. J. 2003, J. Phys. B, 36, 4367
Bates, D. R., Kingston, A. E., & McWhirter, R. W. P. 1962, Proc. R. Soc. London A, 267, 297
Bryans, P., Badnell, N. R., Gorczyca, T. W., Laming, J. M., Mitthumsiri, W., & Savin, D. W. 2006, ApJS, 167, 343
Burgess, A. 1964, MmRAS, 69, 1
Burgess, A., & Summers, H. P. 1969, ApJ, 157, 1007
Butler, K., & Mendoza, C. 1983, J. Phys. B, 16, L707
Butler, K., & Zeippen, C. J. 1990, A&A, 234, 569
Cowan, R. D. 1981, The Theory of Atomic Structure and Spectra (Berkeley: Univ. California Press)
Cunto, W., Mendoza, C., Ochsenbein, F., & Zeippen, C. J. 1993, A&A, 275, L5
Ditchburn, R. W., & Marr, G. V. 1953, Proc. Phys. Soc. A, 66, 665
Fano, U., & Cooper, J. W. 1968, Rev. Mod. Phys., 40, 441
Fu, J., Gorczyca, T. W., Nikolic, D., Korista, K., Badnell, N. R., & Savin, D. W. 2006, Phys. Rev. A, submitted
Garnett, D. R., & Dinerstein, H. L. 2001, ApJ, 558, 145
Gorczyca, T. W., Dumitriu, I., Hasoğlu, Korista, K. T., Badnell, N. R., Savin, D. W., & Manson, S. T. 2006, ApJ, 638, L121
Gould, R. J. 1978, ApJ, 219, 250
Gu, M. F. 2003, ApJ, 589, 1085
Mazzotta, P., Mazzitelli, G., Colafrancesco, S., & Vittorio, N. 1998, A&AS, 133, 403
Nahar, S. N. 1999, ApJS, 120, 131
Péquignot, D., Petitjean, P., & Boisson, C. 1991, A&A, 251, 680
Pindzola, M. S., & Badnell, N. R. 1990, Phys. Rev. A, 42, 6526
Pindzola, M. S., Badnell, N. R., & Griffin, D. C. 1992, Phys. Rev. A, 46, 5725
Shull, J. M., & van Steenberg, M. 1982, ApJS, 48, 95; erratum 1982, ApJS, 49, 351
Storey, P. J. 1994, A&A, 282, 999
Summers, H. P. 2005, ADAS Manual v2.7, http://adas.phys.strath.ac.uk
Summers, H. P., & Hooper, M. B. 1983, Plasma Phys. Control. Fusion, 44, B323
Summers, H. P., et al. 2006, Plasma Phys. Control. Fusion, 48, 263
Verner, D. A., & Ferland, G. J. 1996, ApJS, 103, 467
Verner, D. A., & Yakovlev, D. G. 1995, A&AS, 109, 125
Zatsarinny, O., Gorczyca, T. W., Fu, J., Korista, K. T., Badnell, N. R., & Savin, D. W. 2006, A&A, 447, 379
Zatsarinny, O., Gorczyca, T. W., Korista, K. T., Badnell, N. R., & Savin, D. W. 2004, A&A, 417, 1173 (erratum, 440, 1203 [2005])
Zhang, H. L. 1998, Phys. Rev. A, 57, 2640